Molecular Crystals and Liquid Crystals Science and Technology. Section A. Molecular Crystals and Liquid Crystals

Publication details, including instructions for authors and subscription information:
http://www.tandfonline.com/loi/gmcl19

Time-resolved Total Internal Reflection Raman Scattering Study on Electric-Field-Induced Reorientation Dynamics of Nematic Liquid Crystal of 4-Hexyl-4′-Cyanobiphenyl

T. Morikawa [a] , E. Shirai [a] , J. Tanno [a] , H. Takanashi [b] , A. Yasuda [b] & K. Itoh [a]

[a] Department of Chemistry, School of Science and Engineering, Waseda University, Shinjuku-ku, Tokyo, 169, Japan

[b] Sony Corporation Research Center, Fujizuka-cho, Hodogaya-ku, Yokohama, 240, Japan

Version of record first published: 04 Oct 2006

Mol. Cryst. Liq. Cryst., 1998, Vol. 312, pp. 69–94
Reprints available directly from the publisher
Photocopying permitted by license only

Time-resolved Total Internal Reflection Raman Scattering Study on Electric-Field-Induced Reorientation Dynamics of Nematic Liquid Crystal of 4-Hexyl-4′-Cyanobiphenyl

T. MORIKAWA [a], E. SHIRAI [a], J. TANNO [a], H. TAKANASHI [b], A. YASUDA [b] and K. ITOH [a,*]

[a] *Department of Chemistry, School of Science and Engineering, Waseda University, Shinjuku-ku, Tokyo 169, Japan;*
[b] *Sony Corporation Research Center, Fujizuka-cho, Hodogaya-ku, Yokohama 240, Japan*

(Received 18 February 1997; In final form 29 August 1997)

Total internal reflection (TIR) Raman scattering spectroscopy was performed using a cell combined with a high index hemicylindrical substrate and a glass plate with obliquely evaporated SiO alignment layers to study an electric-field-induced reorientation process of 4-*n*-hexyl-4′-cyanobiphenyl (6CB) in a nematic phase. Two types of cells having different director configurations were studied; one has the orientation of the director parallel to the axis of the hemicylinder (*s*-configuration) and the other the director perpendicular to the axis (*p*-configuration). Squared relative Raman scattering tensor components of the LC layer were determined by analyzing the polarized TIR Raman spectra observed for the cells. Time-resolved TIR Raman measurements were performed on the *p*-configuration cell under application of squared electric fields (duration = 10 ms, repetition rate = 10 and 5 Hz, amplitude = 3–8 V) by using a pulsed Nd-YAG laser (λ_{ex} = 532 nm, pulse width = about 15 ns). The results elucidated characteristics of the electric field-induced reorientation dynamics of a layer of the LC molecules (with a thickness of about 50 nm) adsorbed on the evaporated SiO film: (i) Upon application of the electric field with the amplitudes of 3–5 V the director of the surface layer keeps its original orientation for a certain period, although the director of the bulk phase immediately responds to the fields; the period becomes longer as the amplitude decreases, being ca. 4 ms for the amplitude of 5 V and about 6 ms for 3 V: (ii) After switching off the electric fields the surface layer exhibits a rapid recovery process with the time constant for 3–6 ms, which is appreciably shorter than that of the bulk phase of almost 350 ms (measured under application of the squared electric field of 9 V). An elastic interaction force within the former

*Corresponding author.

layer prevent an immediate response of the LC molecules to the applied electric fields, causing the "induction period". On the other hand, upon switching off the electric fields the interaction force induces a rapid recovery of the director in the surface layer, the time constant of which is independent of the amplitudes of the applied electric fields, and much shorter than the time-constant of the recovery process of the bulk phase.

Keywords: Time-resolved Raman spectroscopy; total internal reflection spectroscopy; electric-field-induced reorientation; nematic liquid crystal; 4-hexyl-4′-cyanobiphenyl

INTRODUCTION

A vast amount of information concerning electric field-induced reorientation dynamics of nematic liquid crystals (LC) such as 4-*n*-pentyl-4′-cyanobiphenyl (5CB) has been accumulated by using various methods including time-resolved infrared [1 – 5] and Raman scattering spectroscopies [6 – 8]. The results indicated a marked difference between the field response of the core part of the cyanobiphenyl moiety and that of the flexible part of the pentyl moeity; the motion of the latter part precedes that of the former at an early stage of the reorientation process [3 – 5]. The time courses of the orientation change elucidated by means of these time-resolved vibrational spectroscopies are mainly associated with the molecules in the bulk phase. In the fabrication process of a nematic LC cell the electrode surfaces are usually covered by a layer of a rubbed polymer such as polyvinyl alcohol and polyimide or by a silicon oxide (SiO) layer prepared by an oblique evaporation technique in order to make either the homogeneous or the homeotropic alignment of the liquid crystal. An anchoring property and/or a morphology of the layer induces a uniaxial orientation of the LC molecules near the electrode surface, which is responsible for the homogeneous or the homeotropic alignment in the bulk phase. Since the anchored molecules require a higher torque for reorientation under an applied electric field, there should be substantial difference in the reorientation dynamics between the molecules near the electrode surface and those in the bulk phase. Although Toriumi [5] inferred such a difference from an intensity change of the C≡N stretching IR band associated with a reorientation process of a 5CB liquid crystal cell after application of a high electric field (20V), there have been no direct experimental data which clarify how the anchoring interaction affects the reorientation dynamics of the surface layer.

In this paper, a total internal reflection (TIR) Raman scattering spectroscopy [9] was applied to study the electric field induced orientation process of a nematic field crystal, 4-*n*-hexyl-4′-cyanobiphenyl (6CB, see Fig. 1), which exhibits the nematic phase in the temperature range of 14 – 29°C.

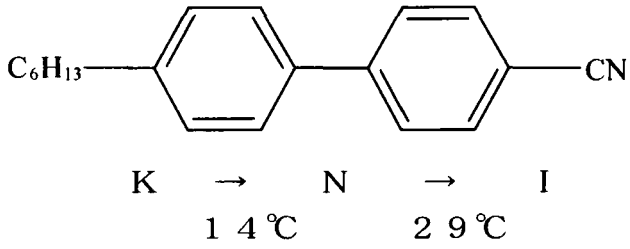

FIGURE 1 Structure of 4-*n*-hexyl-4′-cyanobiphenyl (6CB).

An excitation light source for the TIR Raman scattering spectroscopy is an evanescent wave which is produced in a rarer layer (or a sample layer) by total internal reflection of a laser light shining on the interface between the rarer layer and a denser layer (or a transparent prism with a high refractive index). The penetration depth of the evanescent wave in the sample layer from the interface depends on the angle of incidence, ranging from several decades to several hundreds nanometers for a visible laser excitation light [9]. In the fabrication of the LC cell, we employed the oblique SiO evaporation technique [10] in order to make a homogeneous alignment. The SiO layer with a mass thickness of about 60 nm (see below) is known to have an anisotropic columnar structure [10]. By using a time-resolved TIR Raman spectroscopy we may monitor the reorientation process of the LC layer interacting with the anisotropic structure. In consequence, if we compare the reorientation process of the LC cell probed by the time-resolved TIR Raman spectroscopy with the corresponding processes in the bulk phase probed by a time-resolved transmission IR spectroscopy, it will give insight into the effect of anchoring interactions on the reorientation process of the surface-oriented layer. Based on these considerations, we assembled a time-resolved TIR Raman spectrometer by using a pulsed Nd-YAG laser (pulse width = 15 ns, repetition rate = 10 Hz) and applied it to study the electric-field-induced reorientation process of the nematic LC of 6CB. Time-resolved transmission IR spectroscopic measurements were also performed on a nematic LC cell of 6CB, which was fabricated in the same manner as that employed for the construction of the cells used for the TIR Raman measurements. The results clarified how the response of the surface layer to the electric fields differs from that of the bulk phase, giving insights into the effects of interactions between the LC molecules and the SiO film on the reorientation dynamics.

EXPERIMENTAL

Materials

6 CB was purchased form Tokyo Kasei Co. Ltd. and used as received.

LC Cells

LC cells for TIR Raman measurements were constructed by using a hemicylindrical prism (Schott glass, LaSF08, 15 × 15×7.5 (ϕ) mm, refractive index = 1.888), as shown in Figure 2(A). At the bottom of the prism an indium tin oxide (ITO) layer of a thickness of about 50 nm was made by sputtering, and on the top of the transparent electrode a SiO layer (with a thickness of about 60 nm) was prepared by oblique evaporation of SiO at an incident angle of 60° in order to align the director of the nematic LC of 6CB parallel to the electrode surface [10]. The nematic LC layer with a thickness of ca. 10 μm was sandwiched between the SiO/ITO coating of the high index

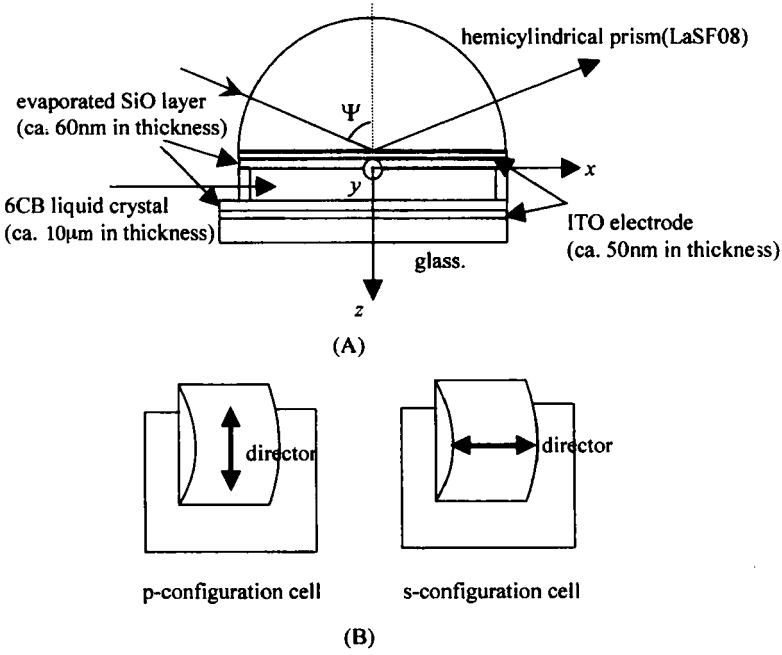

FIGURE 2 Structure of a liquid crystalline cell used for TIR Raman measurements (A) and two kinds of the cell with a different direction of the director (B) (see text).

prism and a transparent electrode, the surface of which also has a layered structure of SiO (about 60 nm)/ITO (about 50 nm)/glass. Two kinds of LC cells were prepared by adjusting the direction of the SiO evaporation (see Fig. 2(B)); *i.e.*, one of the cells has the director parallel to the axis of the hemicylindrical prism and the other has the director perpendicular to the axis; the former cell is called the *s-configuration cell* and the latter the *p-configuration cell*. The average angle between the director and the electrode surface covered by the SiO layer (pretilt angle) was determined by a crystal rotation method [11] to be 0.35°, indicating that the LC molecules in the cells are virtually in homogeneous alignment in the bulk phase.

A liquid crystalline cell for time-resolved IR spectral measurements was fabricated by inserting 6CB into a gap of about 10 μm between two CaF_2 plates (10×10×2 mm), the surface of which was covered by a SiO (about 60 nm)/ITO (about 50 nm) layer prepared in the same manner as that employed by the fabrication of the LC cells for the TIR Raman measurements. The SiO layer made the director of the LC molecules parallel to the cell windows.

Polarized TIR Raman Scattering Measurements of LC Cells with and without Applied Static Electric Fields

TIR Raman spectra of the liquid crystalline cells with and without applied electric fields were recorded by using a Spex Triplemate 1877 spectrometer (f/6.4) equipped with a multichannel detector (Princeton Instrument ICCD-576G/B). A continuous wave argon ion laser (SpectraPhysics model 164) was used as an excitation source ($\lambda = 514.5$ nm). For the TIR Raman measurements under a steady electric-field, an a.c. electric field (5 V, 50 Hz) was applied to the cells by using a function generator (Hokuto Denko model HA-301). Figure 3 illustrates the geometric arrangement of the liquid crystalline cell, an illumination optics of the excitation laser light and a collection optics of Raman scattered light. The excitation laser beam was steered through three rectangular prisms to the hemicylindrical prism with an incident angle Ψ; the polarization of the beam was adjusted to be either parallel (*p*-polarization measurement) or perpendicular (*s*-polarization measurement) to the plane of incidence by using a half-wavelength plate. TIR Raman scattering light was collected from the bottom side of the hemicylindrical prism by a pair of achromatic lens with a focal length of 65 mm and steered to the spectrometer. The Raman scattering component parallel to the axis of the prism (the *y*-component) and that perpendicular to

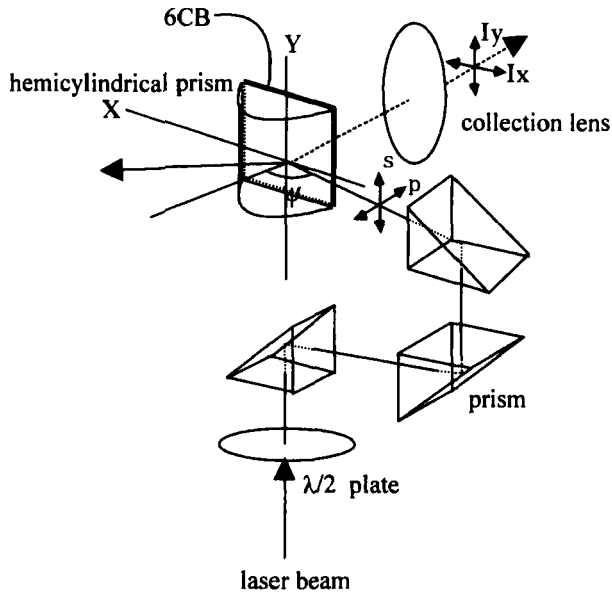

FIGURE 3 Arrangement of a liquid crystalline cell, laser excitation optics and collection optics in the TIR Raman-scattering measurement apparatus.

the axis (the x-component) were recorded by rotating a polarizer, as shown in Figure 3.

Experimental conditions for the TIR Raman measurement under a steady electric field are expressed by an abbreviation such as SPX – 5V; S denotes the s-configuration cell used for the measurement, P indicates the p-polarized laser light for the excitation, X means that the x-component of Raman scattered light was recorded and the figure after the hyphen indicates the amplitude of an a.c. voltage (50 Hz) appleid across the cell.

Time-Resolved TIR Raman Scattering Measurements

Time-resolved Raman scattering measurements were performed by using an apparatus, which consists of a Nd-YAG laser (Spectron Laser Systems model SL404, repetition rate = 5 – 15 Hz, pulse width = 15 ns, $\lambda = 532$ nm), a Kaiser Optical System Holospec f/1.8 spectrometer (f/1.8) equipped with a multichannel detector (Princeton Instruments model ICCD-576G/B) and the optical arrangement in Figure 3. A notch filter at 532 nm (Kaiser Optical System Super Notch-Plus) was used for rejection of stray light around the excitation light. The pulse energy of the excitation laser was reduced to

about 0.4 mJ/pulse in order to avoid damage to the LC cell. The combined use of the highly efficient spectrometer, and the notch filter allows us to record time-resolved TIR Raman spectra within a reasonable accumulation time (at most 15 min); when we measured the spectra by the apparatus employed for the steady state measurements, it took about 1 hour accumulation time. As illustrated by the insert in Figure 9, rectangular electric fields were applied to the LC cells at 5 and 10 Hz by using a Hokuto Denko HA-301 potentiostadt. The amplitude of the field was varied from 3 to 8 V and its duration time was fixed at 10 ms. Firing the excitation pulse laser, applying a rectangular electric field and opening the multichannel detector gate were synchronously triggered by a TTL pulse sequence generated by a pulse generator (Stanford System Research model DG-535).

Time-Resolved Transmission Infrared Spectral Measurements of a LC Cell

Time resolved IR spectra were recorded by using a Bio Rad FTS-60A/896 step scan Fourier transform infrared spectrometer [12] equipped with a DC-coupled linearized MCT detector [13]. A pulsed rectangular electric field (amplitude 3–8 V, duration time 10 ms, repetition rate 10 Hz) was applied to the cell by using a pulse generator (WAVETEK model 75A) and a high-speed power amplifier (NF Electronic Instruments model 404).

RESULTS AND DISCUSSION

Calculation of Electric Field Intensities at the Interface Between the LC and the SiO Layer

The electric field intensities at the interface between the SiO and 6CB layers of the LC cells (Fig. 2) were determined as a function of an incident angle Ψ (the angle of incidence of the excitation laser light in the prism (LaSF08) at the prism/ITO interface) following a usual procedure [14]. The reflectance between the isotropic SiO layer and the anisotropic LC layer was calculated following the procedure of Mosteller and Wooten [15]. The LaSF08, ITO and SiO layers were assumed to be non-absorbing and isotropic with the refractive indices of 1.888, 1.879 and 1.460, respectively [16]. The refractive indices n_e and n_o of the nematic phase of 6CB for the extraordinary and ordinary lights were assumed to be 1.702 and 1.544, respectively [17, 18]. Since the refractive indices of the LaSF08 (prism) and the ITO layer are

similar to each other, we assumed a three-layer structure of prism ($n = 1.88$)/SiO($n = 1.46$)/LC($n_e = 1.702$, $n_o = 1.544$) for the electric field calculation. As shown in Figure 2, the directions of the directors or the optic axes of the nematic LC in the *p*- and *s*-configuration cells are parallel to the *x*- and *y*-axes, respectively. Then, the dielectric permittivity tensor of the LC in the *s*- and *p*-configuration cells are expressed as

$$\varepsilon_0 \begin{pmatrix} n_o^2 & 0 & 0 \\ 0 & n_e^2 & 0 \\ 0 & 0 & n_o^2 \end{pmatrix} \tag{1a}$$

and

$$\varepsilon_0 \begin{pmatrix} n_e^2 & 0 & 0 \\ 0 & n_o^2 & 0 \\ 0 & 0 & n_o^2 \end{pmatrix} \tag{1b}$$

respectively, where ε_0 is the dielectric permittivity under vacuum. On application of an electric field to the *p*-configuration cell the director (or the optic axis) changes its orientation to the direction perpendicular to the electrode surface in the *xz*-plane (Fig. 2). The director rotation angle θ is defined as the angle between the director and the *x*-axis. The dielectric permittivity tensor as a function of θ can be expressed as

$$\varepsilon_0 \begin{pmatrix} n_e^2 \cos^2\theta + n_o^2 \sin^2\theta & 0 & (n_o^2 - n_e^2)\cos\theta\sin\theta \\ 0 & n_o^2 & 0 \\ (n_o^2 - n_e^2)\cos\theta\sin\theta & 0 & n_o^2 \cos^2\theta + n_e^2 \sin^2\theta \end{pmatrix} \tag{2}$$

By using the dielectric permittivity tensors expressed by Eqs. (1) and (2), we calculated the squared electric fields at the LC side of the SiO/6CB interface as a function of the angle of incidence Ψ for the *s*- and *p*-configuration cells; the results are shown in Figure 4. The squared electric fields are normalized to those of the incident light in the high index prism and ITO layer ($n = 1.88$). The results clarify the following points: (i) The critical angle of incidence Ψ_c, which is defined so that, when $\Psi > \Psi_c$, the evanescent wave stands in the LC layer at the 6CB/SiO interface, depends on the kinds of the cells (*p*-configuration or *s*-configuration cell), the polarization of the incident light and the director rotation angle (θ). In the case of the *s*-configuration cell at $\theta = 0°$ Ψ_c is determined to be 55.2° ($= \sin^{-1}(1.544/1.88)$) for the $E_{p,z}^2$ and $E_{p,x}^2$ components and 64.8° ($= \sin^{-1}(1.702/1.88)$) for the $E_{s,y}^2$ component. ($E_{p,i}(i = x, z)$ denotes the *i*-

component of the evanescent electric field at the interface for the p-polarization light and $E_{s,y}$ the y-component of the evanescent electric field for the s-polarized light). In the case of the p-configuration cell ($\theta = 0°$) Ψ_c for the $E^2_{p,z}$, $E^2_{p,x}$ and $E^2_{s,y}$ components are determined to be 55.2°. At $\theta = 90°$ for the s- and p-configuration cells Ψ_c for the E^2_{sy} component is 55.2°, while Ψ_c for the $E^2_{p,z}$ and $E^2_{p,x}$ components is 64.8°. Thus, in the case of the p-configuration cell Ψ_c for the $E^2_{p,z}$ component changes from 55.2 to 64.8°, as the director changes its tilt angle (θ) from 0 to 90°: (ii) The $E^2_{p,x}$ component at $\Psi > \Psi_c$ for both the p- and s-configuration cells are appreciably smaller than the other components: (iii) The components $E^2_{p,z}$

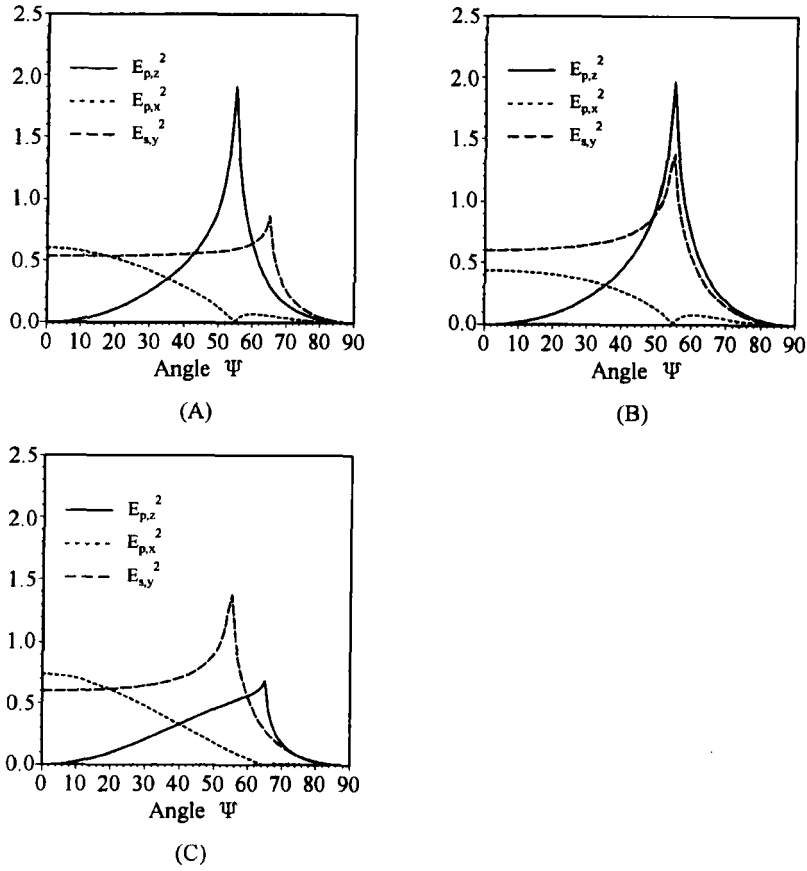

FIGURE 4 Squared relative field intensities at the interface between the nematic phase and the SiO layer as a function of the incidence angle Ψ. (A) s-configuration cell with the director rotation angle (θ) = 0°; (B) p-configuration cell with $\theta = 0°$; (C) p - (or s-) configuration cell with $\theta = 90°$ (see text).

and $E^2_{s,y}$ maximize at Ψ_c and decrease precipitously at $\Psi > \Psi_c$ for both the *s*- and *p*-configuration cells: (iv) The $E^2_{s,y}$ component in the *p*-configuration cell is constant irrespective of the director angle θ, while the $E^2_{p,z}$ and $E^2_{p,x}$ components depend of the director angle. The result (iii) indicates that the TIR Raman measurement should be done by fixing Ψ larger than Ψ_c and as close as possible to Ψ_c and the result (iv) indicates that, when we perform time-resolved TIR Raman spectral measurement by using *s*-polarized excitation laser light for the *p*-configuration cell, the time-course of the scattering intensity can be interpreted only by the rotation of the Raman scattering tensor as the director rotates. This will be explained later in more detail.

TIR Raman Spectra of LC Cells Under Static Field-Off as well as Static Field-On Conditions

Figure 5 shows the TIR Raman scattering spectrum measured under the condition of PPX-0V at $\Psi = 55.5°$. The Raman bands at 2226, 1606, 1280 and 1175 cm^{-1} are ascribable mainly to CN stretching, benzene-ring stretching, inter-ring C—C stretching and CH in-plane bending vibrations, respectively [19].

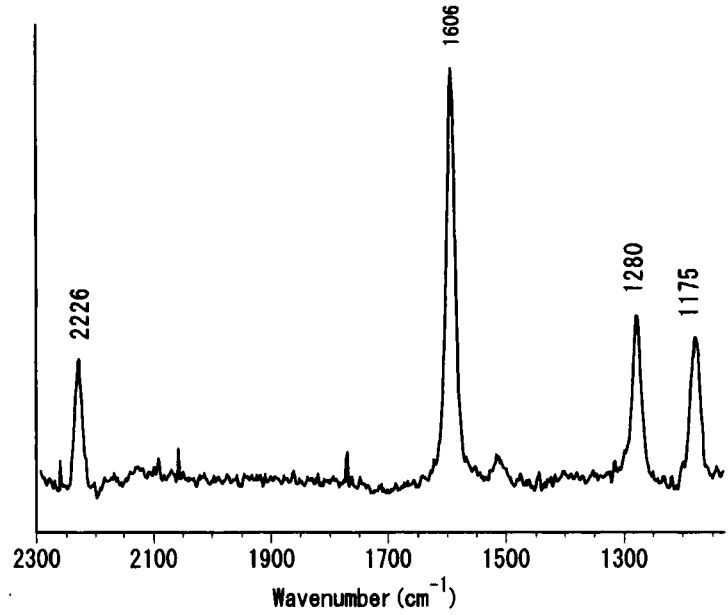

FIGURE 5 The TIR Raman spectrum of 6CB measured under the condition of PPX-0V at $\Psi = 55.5°$.

Figure 6 plots the relative intensities of each Raman band against the angle of incidence Ψ for the *s*-configuration cell under various experimental conditions. The intensities are normalized to the intensity of the 1606-cm^{-1} band observed for the SSY-0V condition at $\Psi = 58°$. The trends of the Ψ-dependence of the Raman bands are similar to each other, which can be ascribed to the fact that an effective symmetry to which the Raman bands belong is virtually identical. Although the intensities of Raman bands are a complicated function of the excitation electric field, the penetration depth of the excitation laser light, and Raman scattering tensor components, as discussed in the next section, there exists a rough correspondence between the plots in the region $\Psi > \Psi_c$ and the calculated electric field intensities summarized in Figure 4A. That is, as Figure 6A and Figure 6B show, the

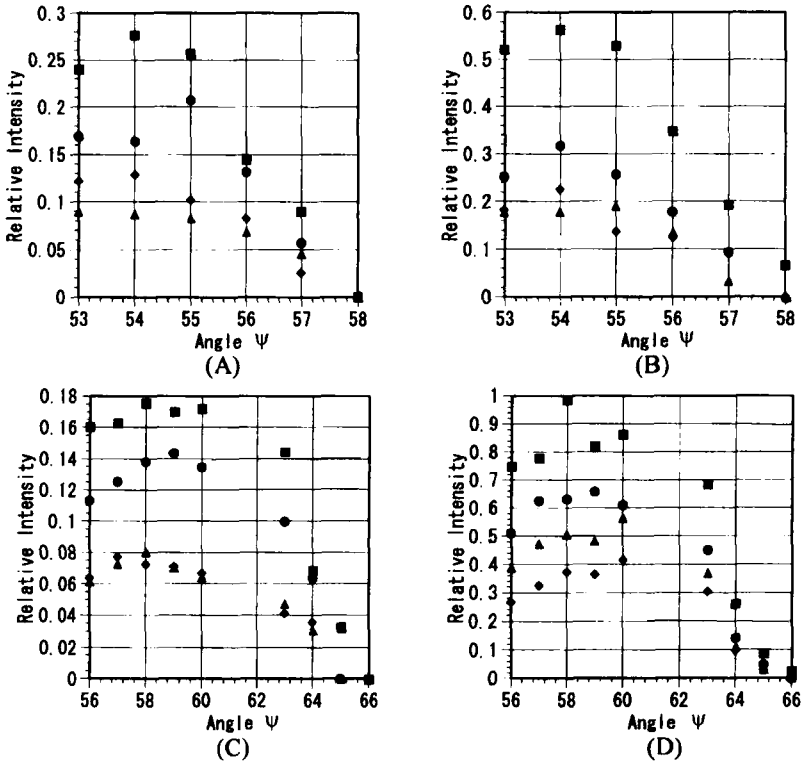

FIGURE 6 Relative intensity changes of the TIR Raman bands of 6CB in the *s*-configuration cell against the angle of incidence Ψ (see text). ■ 1606 cm^{-1}, ● 1280 cm^{-1}, ▲ 1175 cm^{-1}, ◆ 2226 cm^{-1} (A) measured under the condition of SPX-0V; (B) SPY-0V, (C) SSX-0V, (D) SSY-0V.

intensities observed by the *p*-polarized excitation give a maximum in the 54–55° region, which corresponds to the $E^2_{p,z}$ giving the maximum at 55.2° in Figure 4A. The Raman intensities observed by the *s*-polarized excitation (Figs. 6C and 6D) show a broad maximum in the region of 58–62° and a rapid intensity dercease in the region of Ψ larger than 64°, which corresponds to the Ψ-dependence of $E^2_{s,y}$ in Figure 4A.

Figure 7 plots the relative intensities of the Raman bands excited by the *s*-polarized laser light against the angle of incidence Ψ for the *p*-configuration cell. The intensities are normalized to the intensity of the 1606-cm^{-1} band observed for the PSY-5V configuration at $\Psi = 54°$. The Raman scattering intensity profiles observed under the PSX-0V (Fig. 7A) and PSY-0V

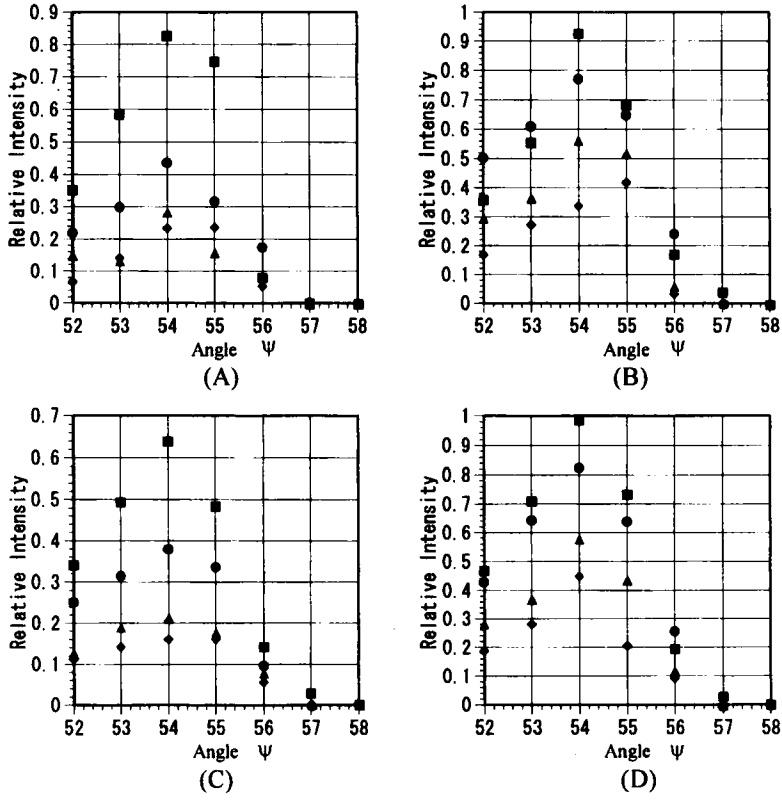

FIGURE 7 Relative intensity changes of the TIR Raman bands of 6CB in the *p*-configuration cell against the anlge of incidence Ψ (see text). The symbols in the figure are the same as those of Figure 6. (A) measured under the condition of PSX-0V; (B) PSY-0V, (C) PSX-5V, (D) PSY-5V.

(Fig. 7B) conditions correspond to the field intensity profiles of the $E^2_{s,y}$ component in Figure 4B, showing a maximum in the 54–55° region and a precipitous decrease in the region of Ψ larger than 55°. As already explained, the electric field intensity of the $E^2_{s,y}$ component in the *p*-configuration cell does not depend on the direction of the director (Figs. 4B and 4C). This was experimentally confirmed because the intensity profiles measured under the condition of PSY-0V (Fig. 7B) are virtually identical with those for the PSY-5V condition (Fig. 7D).

Figure 8 plots the relative intensities of the Raman bands excited by the *p*-polarized laser light against the angle of incidence Ψ for the *p*-configuration cell. The intensities are normalized to the intensity of the 1606-cm^{-1} band

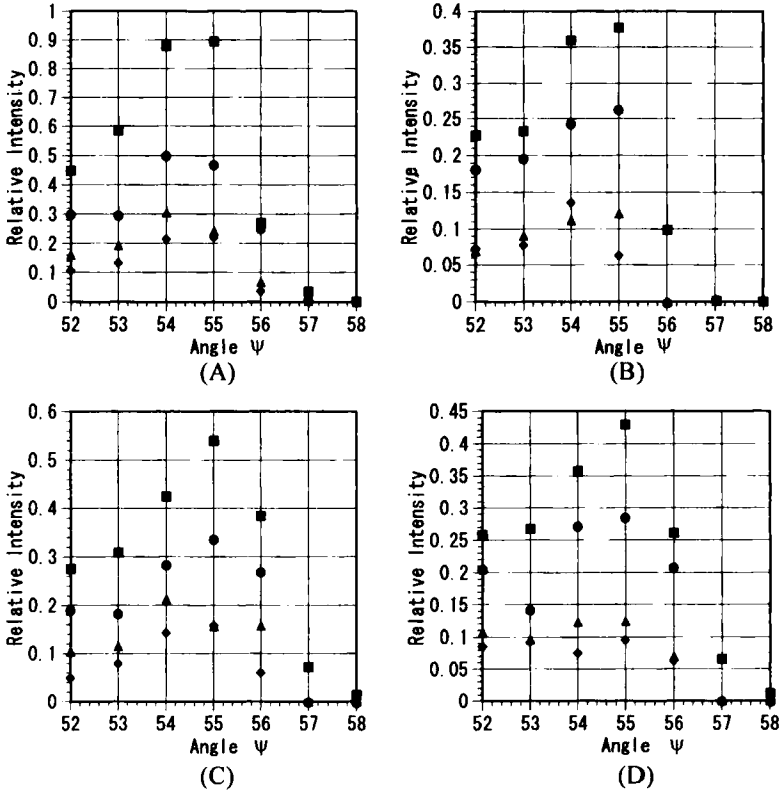

FIGURE 8 Relative intensity changes of the TIR Raman bands of 6CB in the *p*-configuration cell against the angle of incidence Ψ (see text). The symbols in the figure are the same as those of Figure 6. (A) measured under the condition of PPX-0V; (B) PPY-0V, (C) PPX-5V, (D) PPY-5V.

observed for the condition of PSY-5V at $\Psi = 54°$ as in the case of Figure 7. From Figures 8A and 8B, it is clear that the Raman scattering intensity profiles observed under the PPX-0V and PPY-0V conditions correspond to the field intensity profile of the $E_{p,z}^2$ component in Figure 4B, showing a maximum in the 54–55° region and a precipitous decrese in the region of Ψ larger than 55°. Comparing the intensity profiles measured under the PPX- and PPY-0V conditions (Figs. 8A and 8B) with the corresponding profiles measured under the PPX- and PPY-5V conditions (Figs. 8C and 8D), we can recognize that, when the electric field is on, the maximum of the Raman scattering intensity profiles shifts to the larger incidence angle side. As Figures 4B and 4C show, when the director angle θ increases, the profile of the $E_{p,z}^2$ component shifts its maximum to the larger angle side. This result corresponds to the above-mentioned experimental observation.

Determination of Raman Scattering Tensor Components

The nematic phase of 6CB has a uniaxial symmetry along the director (the optical axis). Then, we assumed that, when the electric field is off, the Raman scattering tensor of 6CB can be expressed by the following form:

$$\begin{pmatrix} \alpha_2 & \alpha_3 & \alpha_4 \\ \alpha_3 & \alpha_1 & \alpha_3 \\ \alpha_4 & \alpha_3 & \alpha_2 \end{pmatrix} \tag{3}$$

for the *s*-configuration cell (the director is parallel to the *y*-axis; see Fig. 2), and

$$\begin{pmatrix} \alpha_1 & \alpha_3 & \alpha_3 \\ \alpha_3 & \alpha_2 & \alpha_4 \\ \alpha_3 & \alpha_4 & \alpha_2 \end{pmatrix} \tag{4}$$

for the *p*-configuration cell. Here, α_1 and α_2 are diagonal components corresponding to the direction parallel and perpendicular, respectively, to the director, and α_3 and α_4 are cross terms. By using these tensor components the Raman scattering intensities observed under the electric field-off condition (i.e., $\theta = 0°$) can be expressed by the following equations;

$$I_{SSX} = A_{SS}\,\alpha_3^2\langle E_y\rangle^2, \quad I_{SSY} = A_{SS}\,\alpha_1^2\langle E_y\rangle^2 \tag{5a}$$

$$I_{SPX} = A_{SP}\,(\alpha_2\langle E_x\rangle + \alpha_4\langle E_z\rangle)^2, \quad I_{SPY} = A_{SP}\,(\alpha_3\langle E_x\rangle + \alpha_3\langle E_z\rangle)^2 \tag{5b}$$

$$I_{PSX} = A_{PS}\,\alpha_3^2\langle E_y{}^2, \quad I_{PSY} = A_{PS}\,\alpha_2^2\langle E_y\rangle^2 \tag{5c}$$

$$I_{PPX} = A_{PP}(\alpha_1\langle E_x\rangle + \alpha_3\langle E_z\rangle)^2, \quad I_{PPY} = A_{PP}(\alpha_3\langle E_x\rangle + \alpha_4\langle E_z\rangle)^2 \qquad (5d)$$

where $I_{\eta\rho\xi}$ is the relative Raman-scattering intensity observed for the configuration η (p- or s-configuration cell), ρ (p- or s-polarized excitation light) and ξ (the Raman scattering intensity component parallel to the x- or y-axis). In Eqs. (5a)–(5d) $\langle E_i\rangle$ ($i = x, y, z$) expresses an i-th component of an effective electric field of the evanescent wave within an LC-layer near the 6CB/SiO interface, in which Raman scattering is taking place, and $A_{\eta\rho}$ is a constant determined by the cell configuration η and the polarization of the excitation laser light ρ. $\langle E_i\rangle$ ($i = x, y, z$) was assumed to be equal to the calculated electric fields at the 6CB/SiO interface shown in Figure 4. From Eqs. (5a) and (5c) we can obtain the following equations.

$$\frac{I_{SSY}}{I_{SSX}} = \frac{\alpha_1^2}{\alpha_3^2}, \quad \frac{I_{PSY}}{I_{PSX}} = \frac{\alpha_2^2}{\alpha_3^2} \qquad (6a)$$

As can be seen from Figure 4, $E_{p,x}^2$ is far smaller than $E_{p,z}^2$ at Ψ near Ψ_c($\Psi > \Psi_c$) both for the s- and p-configuration cells. Then, we assumed that $\langle E_x\rangle$ is negligible compared to $\langle E_z\rangle$ in Eqs. (5b) and (5d), which gives the Eq. (6b). (This assumption, however, is not always correct, as discussed below).

$$\frac{I_{SPX}}{I_{SPY}} = \frac{I_{PPY}}{I_{PPX}} = \frac{\alpha_4^2}{\alpha_3^2} \qquad (6b)$$

From the experimental results summarized in Figures 6–8 and Eqs. (6a) and (6b), we can determine the following values $(\alpha_1/\alpha_3)^2$, $(\alpha_2/\alpha_3)^2$ and $(\alpha_4/\alpha_3)^2$, which are listed in Table I. The scattering intensities observed for each Raman band measured under the conditions, SSX- and SSY-0V at $\Psi = 64°$, and the other conditions at $\Psi = 55°$ were employed for the determination. (Although the angles (64 and 55°) are slightly smaller than the critical angles calculated for the corresponding conditions (55.2 and 64.8°, vide supra), we confirmed that total reflection takes place at these angles by performing reflectance measurements. The discrepancy may be due to the assumption that the 6CB/SiO interface forms an ideal flat surface.) The $(\alpha_4/\alpha_3)^2$ values determined from I_{SPX}/I_{SPY} and I_{PPY}/I_{PPX} are slightly different from each other. For example, the value for the 1606-cm^{-1} band determined from I_{SPX}/I_{SPY} is 0.52, while the value from I_{PPY}/I_{PPX} is 0.46. This may be due to the assumption that $\langle E_x\rangle = 0$. The values listed in Table I are taken from the average of the $(\alpha_4/\alpha_3)^2$ values determined from I_{SPX}/I_{SPY} and those from

TABLE I Squared ratios of the Raman scattering tensor components

	1175 cm^{-1}	*1280 cm*$^{-1}$	*1606 cm*$^{-1}$	*2226 cm*$^{-1}$
α_1^2/α_3^2	3.76	2.35	3.84	2.94
α_2^2/α_3^2	3.12	2.00	0.92	2.94
α_4^2/α_3^2[a]	0.49	0.54	0.49	0.57

[a] The average of α_4^2/α_3^2 values determined from I_{SPX}/I_{SPY} and those from I_{PPY}/I_{PPX} (see text).

I_{PPY}/I_{PPX}. This does not affect the main conclusion of this paper, as explained in the next section.

Time-Resolved TIR Raman Spectra of the *p*-Configuration Cell

On application of an electric field across the *p*-configuration cell the Raman scattering tensor changes as a function of the director rotation angle θ in accordance with the following formula,

$$\begin{pmatrix} \alpha_{xx} & \alpha_3\cos\theta + \alpha_4\sin\theta & \alpha_{xz} \\ \alpha_3\cos\theta + \alpha_4\sin\theta & \alpha_2 & -\alpha_3\sin\theta + \alpha_4\cos\theta \\ \alpha_{xz} & -\alpha_3\sin\theta + \alpha_4\cos\theta & \alpha_{zz} \end{pmatrix} \quad (7)$$

where α_{xx}, α_{xz} and α_{zz} are defined as

$$\alpha_{xx} = \alpha_1\cos^2\theta + \alpha_2\sin^2\theta + 2\alpha_3\cos\theta\sin\theta \quad (8a)$$

$$\alpha_{xz} = -(\alpha_1 - \alpha_2)\cos\theta\sin\theta + \alpha_3(\cos^2\theta - \sin^2\theta) \quad (8b)$$

$$\alpha_{zz} = \alpha_1\sin^2\theta + \alpha_2\cos^2\theta - 2\alpha_3\cos\theta\sin\theta \quad (8c)$$

By using the tensor components in equation (7), the Raman scattering intensity measured for the *p*-configuration cell under each condition at the director rotation anlge θ, can be expressed as follows;

$$I_{PPX} = A'_{PP}(\alpha_{xx}\langle E_x\rangle + \alpha_{xz}\langle E_z\rangle)^2 \quad (9a)$$

$$I_{PPY} = A'_{PP}\left\{(\alpha_3\cos\theta + \alpha_4\sin\theta)\langle E_x\rangle + (-\alpha_3\sin\theta + \alpha_4\cos\theta)\langle E_z\rangle\right\}^2 \quad (9b)$$

$$I_{PSX} = A'_{PS}(\alpha_3\cos\theta + \alpha_4\sin\theta)^2\langle E_y\rangle^2 \quad (9c)$$

$$I_{PSY} = A'_{PS}\alpha_2^2\langle E_y\rangle^2 \quad (9d)$$

where $A'_{\eta\rho}$ is a constant determined by the cell configuration η (*p*- or *s*-configuration) and the polarization of the excitation laser light ρ (*p*- or

s-polarization). As already explained, the squared electric field amplitude at the 6CB/SiO interface $\langle E_Y \rangle^2$ does not depend on the director rotation angle θ. Then, equations (9c) and (9d) indicate the following facts; (i) I_{PSX} depends only on the rotation angle θ, (ii) I_{PSY} is independent of θ and constant. In this paper the ratio

$$\frac{I_{PSX}}{I_{PSY}} = \frac{(\alpha_3 \cos\theta + \alpha_4 \sin\theta)^2}{\alpha_2^2} \tag{10}$$

was measured and related to θ, by using the values of $(\alpha_3/\alpha_2)^2$ and $(\alpha_4/\alpha_2)^2$ taken from those in Table I.

Figure 9 illustrtates the time-resolved TIR Raman scattering spectra measured under the PPX condition at $\Psi = 56°$. As expressed by the inserted figure, the periodic rectangular electric field (8 V, 10 ms duration, 10 Hz) was applied across the p-configuration cell for the measurement. The spectra are shown as a function of time after the application of the rectangular electric field.

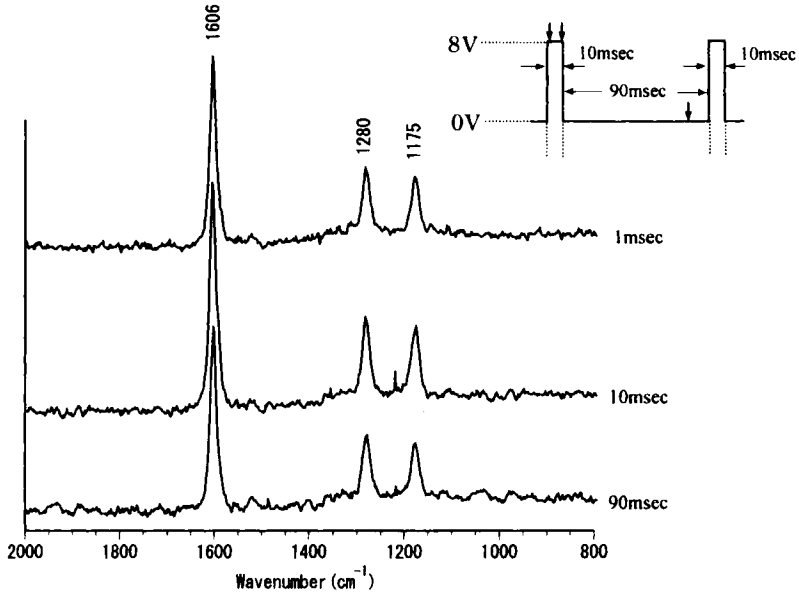

FIGURE 9 The time- resolved TIR Raman spectra of 6CB in the p-configuration cell measured under the condition of PPX at $\Psi = 56°$ with the applied periodic electrode potential (10 ms duration, 10 Hz) depicted by the insert. Each spectrum was measured at the time after application of the electric field. The time is indicated by a vertical arrow in the insert (see text).

Figure 10 plots the time-course of the relative Raman scattering intensity change at 1606 cm^{-1} observed under various conditions for the *p*-configuration cell in the time range of 0–20 ms. All the intensities are normalized to that observed at $t=90$ ms under the PSX condition. The relative intensity observed under the PSY condition (Fig. 10B) is virtually constant in the time range; as equation (9d) shows, I_{PSY} is proportional to $\langle E_y \rangle^2$ with a constant proportionality factor of $A'_{PS}\alpha_2^2$. Then, the above-mentioned result experimentally proves the independence of $\langle E_y \rangle^2$ on the

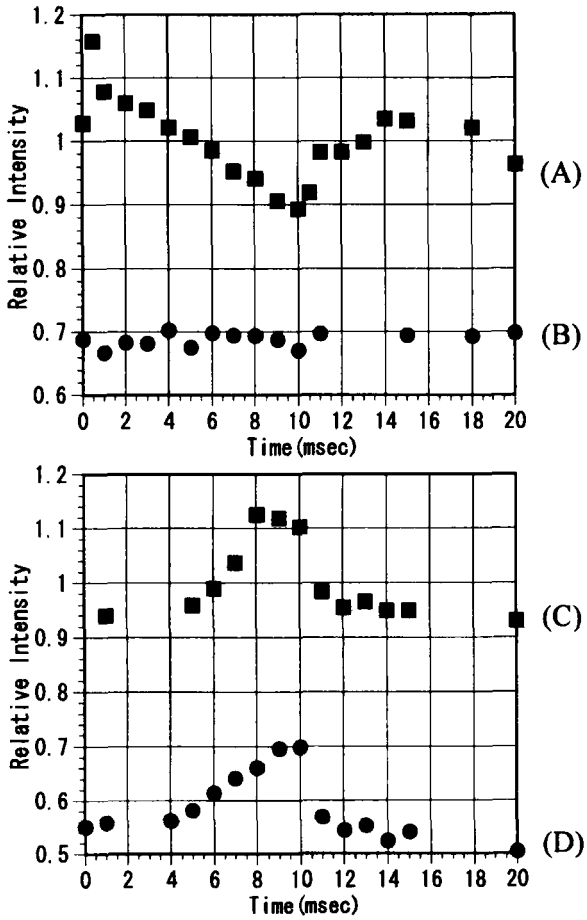

FIGURE 10 The relative intensity change of the TIR Raman band at 1606 cm^{-1} during the application of the periodice electric field of 8 V (10 ms duration, 10 Hz) measured for the *p*-configuration cell at $\Psi = 56°$ under the conditions of (A) PSX, (B) PSY, (C) PPX and (D) PPY (see text).

director rotation. The relative intensity observed under the PSX, PPX and PPY conditions (Figs. 10A, 10C and 10D) shows appreciable change; the change in the time range of 0 – 10 ms reflects the director rotation away from a parallel alignment on the electrode surface, and the change in the range of 10 – 20 ms the recovery process of the director reorientation. Since α_{xx} and α_{xz} are functions of θ through Equation (8a) and (8b) and $\langle E_x \rangle$ and $\langle E_z \rangle$ depend of θ, equations (9a) and (9b) indicate that the changes measured under the conditions PPX and PPY conditions (Figs. 10C and 10D) are also complicated functions of θ. On the other hand, since $\langle E_y \rangle^2$ is constant irrespective of θ, as experimentally proved, the changes measured under the PSX condition (Fig. 10A) can be used to determine the time course of the director rotation angle θ by using equation (10). The result is summarized by solid circles in Figure 11A together with the time course of the director rotation determined in a similar manner by applying the electric fields with the amplitudes of 5 and 3V at 10 Hz (open circles and solid triangles in Fig. 11A). Figure 11B summarizes the time courses of the director rotation angle, which are determined by applying the electric fields with the amplitude of 5 and 8 V at 5 Hz. (As mentioned in the previous section, there is an ambiguity in the experimentally determined $(\alpha_4/\alpha_3)^2$ values. However, a change of the value for the 1601-cm^{-1} band within ± 0.03 does not affect the over-all features of the director rotation angle changes in Fig. 11.) Figure 11 clearly indicates that, upon application of the electric fields with the amplitude of 3 to 8 V with the duration of 10 ms, the director changes its initial rotation angle (about 20° at 10 Hz and about 15° at 5 Hz) to a maximum value at 10 ms, and, upon switching off the applied field, the director recovers the initial rotation angle. The initial director rotation angles are appreciably different from that of the bulk phase, which is virtually zero, as explained in the experimental section. Presumably, a rectangular electric field applied to the cell may induce an electrochemical process, resulting in an accumulation of charged species near the electrode surface [20]. Although a discharging may take place during the period of zero electric field, it is not completed during the period (90 ms at 10 Hz and 190 ms at 5 Hz) and the remaining charges may effect the initial director rotation away from the electrode surface. The smaller initial rotation angle observed at 5 Hz compared to that at 10 Hz conforms to this reasoning, because the extent of the discharge at 5 Hz is expected to be larger than that at 10 Hz.

The following facts are also clarified from Figure 11.

(1) The response process of the director to the application of the electric field depends on the field amplitude; that is, the director responds almost

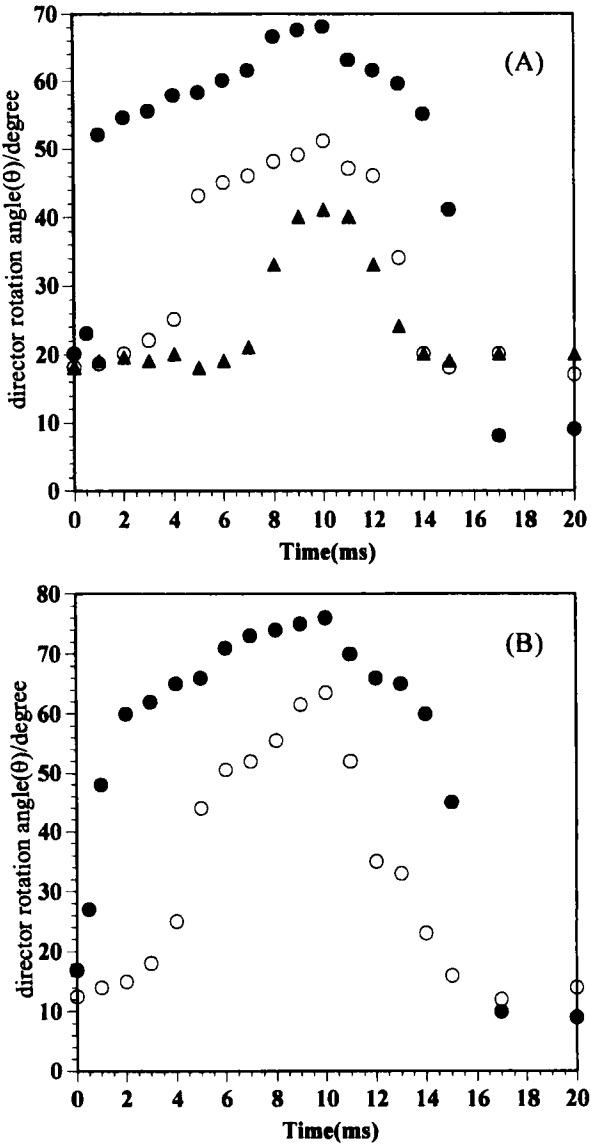

FIGURE 11 Director rotation angle change in the surface layer as a function of time after application of the electric field (10 ms duration) with various amplitudes at 10 Hz (A) and at 5 Hz (B). (A) ● the amplitude of the electric field = 8 V, ○ 5 V, ▲ 3 V (B) ● 8 V, ○ 5 V.

immediately to the applied field of 8 V, the response being completed virtually within 1–2 ms (solids circles in Figs. 11A and 11B), while upon application of the fields of 5 and 3 V there occurs an induction period in

which the director does not responds to the field (open circles and closed triangles in Figs. 11A and 11B). The period becomes longer as the applied electric field decreases; i.e., about 4 ms for the field of 5 V and about 6 ms for the field of 3 V. Presumably, the period exists also for the response process at the applied field of 8 V. It is, however, too short (less than 1 ms) to be experimentally determined.

(2) Upon switching off the electric field (at 10 ms), the director changes its orientation to the initial rotation angle within about 6 ms. The time constant and the mode of the recovery process do not depend on the applied electric field in the range of 3–8 V.

(3) The final director rotation angle (at 10 ms) at the applied field of 8 V is appreciably larger than those at 5 and 3 V.

(4) The response behavior of the director to the applied field does not depend on the repetition cycles (10 or 5 Hz) except for the initial director rotation angle. (The director rotation angle vs. time plots in Figure 11A seem to differ slightly from those in Figure 11B. The difference, however, cannot be considered to reflect a real situation).

In order to check whether the results summarized above are characteristic features of the LC molecules near the SiO film, we performed time-resolved transmission IR spectral measurements on an LC cell which was fabricated in the same manner as that employed to make the cells for the TIR Raman measurements.

Time-Resolved Transmission IR Spectra of a LC Cell

Figure 12 shows the static polarized transmission IR spectra of the LC cell, measured with the polarized parallel (A) and perpendicular (B) to the director in the homogeneous alignment. The dichroic ratio of 2.97 observed for the C≡N stretching band at 2227 cm^{-1} and that of 3.26 for the benzene ring stretching band at 1606 cm^{-1} are close to the corresponding ratios observed for a nematic 5CB liquid cell [1]. The time-resolved transmission IR spectra were recorded for the LC cell under the periodic electric field with an amplitude of 3–8 V at 10 Hz. (The field with the amplitude of 8 V at 10 Hz is illustrated by the insert in Fig. 9). The polarizer was put parallel to the original director orientation in the homogeneous alignment. Upon application of an electric field an IR band, the transition moment of which is parallel to the director, reduces its intensity. Figure 13 summarizes the intensity changes of 1606 cm^{-1} IR band under the application of the periodic fields. When normalized to the intensity at 0 ms, the relative

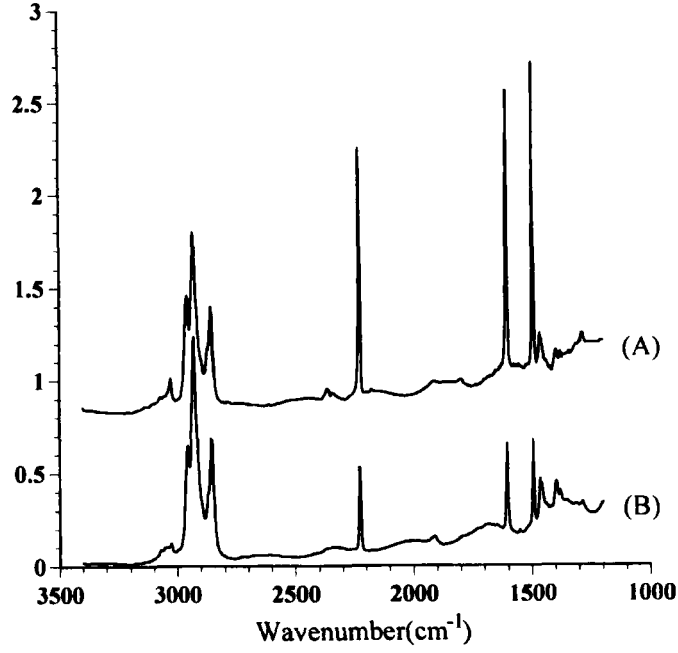

FIGURE 12 Polarized IR spectra of 6CB measured with the direction of polarization of IR light parallel (A) and perpendicular (B) to the director of the cell.

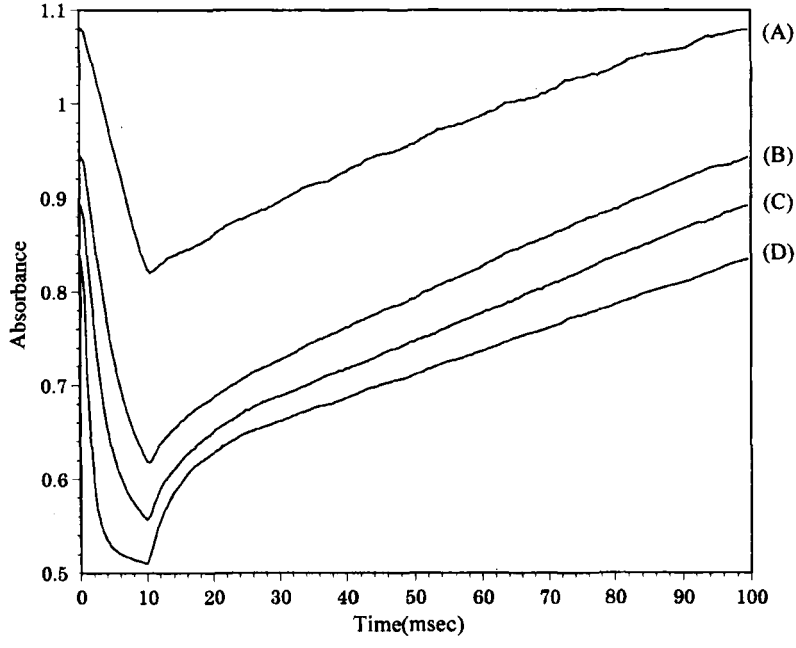

FIGURE 13 Intensity change (in absorbance scale) of the 1606 cm^{-1} IR band as a function of time after application of electric fields (10 ms duration, 10 Hz) with the amplitudes of 3 V (A), 4 V(B), 5 V(C) and 8 V(D).

intensity changes of the 1606 and 2227 cm^{-1} bands coincide with each other, indicating that the average directions of the transition moment of both bands are identical with each other. The absorbance decrease in the range of 0 – 10 ms in Figure 13 reflects the director rotation from a tilted orientation (with a small θ) to a less tilted one (with a larger θ) and the absorbance increase in the range of 10 – 100 ms reflects the director rotation to an original orientaion. The fact that the absorbance at 0 ms (or at 100 ms) strongly depends on the applied electric fields, however, indicates that the orientation recovery process is not completed at 90 ms after switching off the electric fields. (A preliminary measurement indicated that upon application of the field of 9 V, the complete recovery requires almost 350 ms).

The angle $\theta'(t)$ between the transition moment of the 1606 cm^{-1} band and the electrode surface of the cell can be calculated as a function of time after application of the electric field through the following equation,

$$\theta'(t) = \cos^{-1}\sqrt{\left\{\frac{(A(t) - A_\perp)}{(A - A_\perp)}\right\}} \tag{11}$$

where $A(t)$ indicates the absorbance measured at time t and A and $A_\perp$ are defined by the absorbance of the band measured under ideal homogeneous and homeotropic alignment conditions, respectively. Assuming A and $A_\perp$ to be equal to the absorbance of the IR band in the polarized IR spectra measured with the polarizer parallel and perpendicular, respectively, to the director, we applied equation (11) to calculate $\theta'(t)$ from the absorbance change summarized in Figure 13. The results for the applied electric field amplitudes of 3, 5 and 8 V at 10 Hz are shown in Figure 14. Assuming that $\theta'(t)$ is equal to the director rotation angle discussed in the preceding sections, we can recognize the following facts from the figure:

(1) The director rotation angle in the bulk phase at 0 ms strongly depends on the applied electric fields, which means that the director does not complete its reorientation process at 90 ms after switching off the applied electric field, as already explained. This is in a marked contrast to the case of the surface layer, where the rotation angle at 0 ms is virtually constant and the recovery process is completed within 5 – 6 ms irrespective of the amplitudes of the electric field (see Fig. 11).

(2) The time constants of the electric field-induced reorientation process in the bulk phase depend on the amplitudes of the electric field, the time constants at 8V being appreciably shorter than those at 5 or 3 V. The over-all features of the reorientation process, however, are similar to

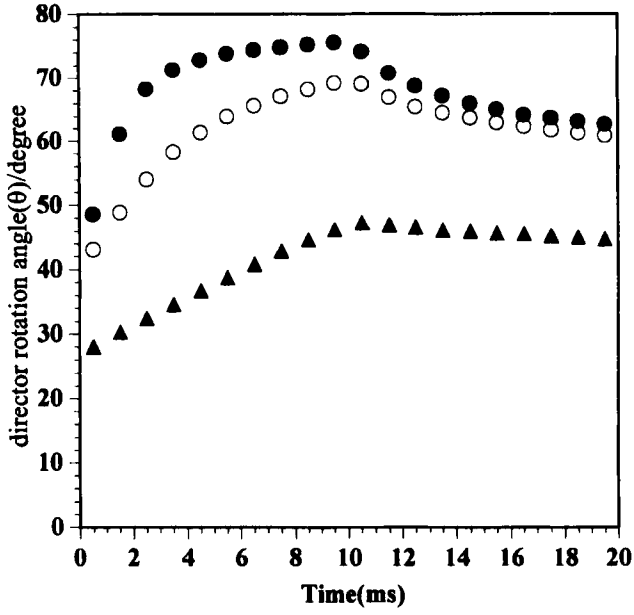

FIGURE 14 Director rotation angle change in the bulk phase as a function of time after application of the electric fields (10 ms duration) at 10 Hz with the amplitudes of 8 V (●), 5 V (○) and 3 V (▲).

each other. Further, the bulk phase does not show any clear induction period, which is observed for the surface layer at the applied electric fields of 5 and 3V (Fig. 11).

(3) The time constants of the recovery process in the bulk phase are much longer than those observed for the LC molecules near the SiO film.

All these results proved that the existence of the induction period and the very fast recovery process with the time constant of 5–7 ms, which is independent of the applied electric fields, are the characteristic features of the electric field-induced orientation dynamics of the surface layer. The oblique evaporation of SiO is known to result in the formation of a grooved or columnar structure, which causes the homogeneous alignment of the LC layer near the surface mainly through an elastic interaction [21]. The interaction exerts itself to suppress an immediate response of the director of the surface layer to the applied electric fields. Presumably, when the director of the molecules in the bulk phase rotates to a certain extent, an attractive force between the bulk phase and the surface layer induces the rotation of the director of the surface layer. On the other hand, when the electric field is

switched off, the elastic interaction, which causes the homogeneous alignment of the surface layer, rapidly drives the director of the surface layer back to its original orientation.

CONCLUSIONS

The time-resolved TIR Raman spectroscopy clearly proved that the elastic interaction, which causes the homogeneous alignment of the surface layer near the obliquely evaporated SiO film, plays a dominant role in the reorientation dynamics of the layer: At an initial stage of the response the interaction force suppresses a rapid response of the molecules to an applied electric field: On the other hand, after the field is switched off, the force causes a rapid recovery of the original director orientation of the surface layer, which takes place independently of the recovery process of the bulk phase. This dynamic behavior monitored by the time-resolved TIR Raman spectroscopy, however, is still average one within the surface layer of the thickness of about 50 nm – the penetration depth of the evanescent excitation light at $\Psi = 56°$. Then, in order to get more detailed insight into the effect of the LC-SiO surface interaction on the dynamic behaviors of the nematic LC cell, we need to perform similar experiments by changing the incidence angle (or the penetration depth).

Acknowledgements

We are grateful to Mr. Shigeru Shimada and Dr. Toru Yokoyama of Nippon BioRad Corporation for measuring the time-resolved IR spectra of the liquid crystalline cell.

References

[1] A. Kaito, Y. K. Wang and S. L. Hsu, *Anal. Chim. Acta.*, **189**, 27 (1986).
[2] H. Toriumi, H. Sugisawa and H.Watanabe, *Japanese J. Appl. phys.*, **27**, L935 (1988).
[3] T. I. Urano and H. Hamaguchi, *Chem. Phys. Lett.*, **195**, 287 (1992).
[4] T. Nakano, T. Yokoyama and H.Toriumi, *J. Appl. Spectry.*, **47**, 1354 (1993).
[5] H. Toriumi, *Mol. Cryst. Liq. Cryst.*, **262**, 371 (1995).
[6] H. J. Coles and J. Tipping, *Nature*, **316**, 136 (1985).
[7] K. M. Booth, J. Nash and H. J. Coles, *Meas. Sci. Tech.*, **3**, 843 (1992).
[8] K. M. Booth and H. J. Coles, *Liquid Cryst.*, **13**, 677 (1993).
[9] R. Iwamoto, M. Miya, K. Ohta and S. Mima, *J. Chem. Phys.*, **74**, 4780 (1981).
[10] J. L. Janning, *Appl. Phys. Lett.*, **21**, 173 (1972).
[11] T. J. Scheffer and J. Nehring, *J. Appl. Phys.*, **48**, 1783 (1977).

[12] R. A. Crocombe and S. V. Compton, *FTS/IR Notes* No. 82 (1991).
[13] R. Curbelo, *United States Patent* No. 5262635 (1993).
[14] M. Born and E. Wolf, *In Principle of Optics*, 6th Edition pp. 36 pp. 55, pp. 665 (1980).
[15] L. P. Mosteller Jr. and F. Wooten, *J. Opt. Soc. Am.*, **58**, 511 (1968).
[16] H. R. Philips in *Handbooks of Optical Constants of Solids*, Academic Press, pp. 746 (1985).
[17] D. Riviere, Y. Levy and C. Imbert, *Optics Comm.*, **26**, 206 (1978).
[18] Y. Levy, D. Riviere, C. Imbert and M. Boix, *Optics Comm.*, **26**, 225 (1978).
[19] G. W. Gray and A. Mosley, *Mol. Cryst. Liq. Cryst.*, **35**, 71 (1976).
[20] C. Colpaert, B. Maximus and H. Pauwels, in *Proceedings of the IDRC 1993*, pp. 301 (1993).
[21] M. B. Feller, W. Chen and Y. R. Shen, *Phys. Rev. A*, **43**, 6778 (1991).